This is a preprint, the final version is subject to change, of the American Mineralogist (MSA)
Cite as Authors (Year) Title. American Mineralogist, in press.
(DOI will not work until issue is live.) DOI: http://dx.doi.org/10.2138/am-2017-5793

REVISION 3

WATER TRANSFER DURING MAGMA MIXING EVENTS: INSIGHTS INTO CRYSTAL MUSH REJUVENATION AND MELT EXTRACTION PROCESSES

Mattia Pistone [1,2], Jon Blundy [1], Richard A. Brooker [1], EIMF [3]

1) *School of Earth Sciences, University of Bristol, Wills Memorial Building, Queen's Road, BS8 1RJ, Bristol, United Kingdom.*
2) *Department of Mineral Sciences, National Museum of Natural History, Smithsonian Institution, 10th Street & Constitution Avenue NW, Washington, DC 20560-0119, United States.*
3) *Edinburgh Ion Microprobe Facility, School of Geosciences, University of Edinburgh, Grant Institute, Kings Buildings, West Mains Road, EH9 3JW, Edinburgh, United Kingdom.*

Abstract

Many plutons preserve evidence of magma mixing between hydrous mafic magmas and resident felsic crystal-rich mushes. To investigate water transfer processes in such systems following thermal equilibration, we conducted 24-hour experiments to establish the petrological evolution of a water-undersaturated (4 wt% H_2O in the interstitial melt) quartz-bearing dacite crystal mush (0.5-0.8 in crystal fraction) intruded by a water-saturated (≥ 6 wt% H_2O), initially crystal-free, andesite magma at 950 °C and 4 kbar (12 km depth). Our results show isothermal undercooling resulting from a change in liquidus temperatures of the interacting magmas due to their changing water content. Specifically, mafic samples dramatically crystallise during water escape into the felsic end-members and consequent increase in liquidus temperature. Conversely, the addition of water to the felsic mush reduces the liquidus temperature, leading to an increase in melt fraction. The experiments provide insights into how volatiles contribute to crystal mush rejuvenation (i.e.,

Always consult and cite the final, published document. See http:/www.minsocam.org or GeoscienceWorld

increase of melt fraction). However, H_2O diffusion alone is not sufficient to promote melt extraction from short- and long-lived mushes in the Earth's crust.

Introduction

The link between crustal architecture, the fluxes of magma through the crust, and the attendant transfer of heat, mass, and fluid, is fundamental to our understanding of crust-forming processes (e.g., Hildreth and Moorbath 1988; Huppert and Sparks 1988; Barboza and Bergantz 1997; Tatsumi, 2000; Bohrson and Spera 2001; Solano et al. 2012; Dungan and Davidson, 2004; Dufek and Bergantz 2005; Annen et al. 2006; Takahashi et al. 2007; Huber et al. 2009; 2010; Chiaradia et al. 2011; Paterson et al. 2011; Paterson and Ducea 2015). In arc settings in which large volatile budgets are released from the subducting slab (e.g., Ulmer and Trommsdorff 1995; Poli and Schmidt 1995; Schmidt and Poli 1998), the Earth's continental crust is a processing zone, fed by mantle-derived, hydrous magmas (H_2O contents of 1-7 wt%, with 4 wt% on average; Ulmer 2001; Plank et al. 2013; CO_2 contents of > 250 ppm; Cervantes and Wallace 2003; Blundy et al. 2010) and releasing H_2O-rich, differentiated (felsic) melts to shallower crustal depths where they degas and crystallise. The resultant felsic crystal mushes (i.e., partially molten rocks between the liquidus and solidus temperatures) are often rheologically stalled bodies with average solid fractions (ϕ) of 0.4-0.6, close to the microstructural transition from a suspension of isolated crystals in a melt to a solid framework containing a through-going network of melt channels (e.g., Lejeune and Richet 1995; Caricchi et al. 2007). Felsic crystal mushes may be thermally stable for long periods of time (Glazner et al. 2004; Caricchi and Blundy 2015); whether they are mobilised to erupt, or solidify to form plutons, is primarily a function of the extent to which they are sustained by further

Always consult and cite the final, published document. See http:/www.minsocam.org or GeoscienceWorld

additions of heat and volatiles. An important process of heat and volatile addition is the injection of hydrous mafic magmas into crystal mushes. Many volcanic rocks carry evidence of mafic injection shortly before eruption, and this process has been invoked as an eruption trigger (e.g., Eichelberger and Izbekov 2000; Murphy et al. 2000; Suzuki and Nakada 2007; Sigmundsson et al. 2010; Tomiya et al. 2013).

Mafic-felsic magma interactions have the potential to remobilise near-solidus felsic crystal mushes by means of heat (Burgisser and Bergantz 2011; Tapster et al. 2016) or volatiles (Bachmann and Bergantz 2006; Parmigiani et al. 2016), or a combination of both (Huber et al. 2011; Parmigiani et al. 2014). Felsic crystal mush "defrosting" (Huber et al. 2010) could be triggered by the percolating buoyant volatiles with a high specific heat, which can assist the reactivation of the mush by allowing significant heat advection. Volatiles are also essential in the rheological rejuvenation of crystal mushes by lowering their viscosity (e.g., McByrne and Murase 1984; Petford 2003; Ardia et al. 2008; Pistone et al. 2013), density (e.g., Ochs and Lange 1999; Bachmann and Bergantz 2004; Malfait et al. 2014; Ardia et al. 2014), and liquidus temperature (e.g., Tuttle and Bowen 1958; Johannes and Holtz 1996; Pistone et al. 2016), reducing the crystal content by partial melting (Huber et al. 2010). Rejuvenation of the mush can be enhanced by high volatile content (> 4 wt% H_2O) in the mafic intrusion and low confining pressure (< 2 kbar; volatile-saturated conditions). However, at lower initial volatile contents (< 4 wt% H_2O) and higher pressure (3-4 kbar; volatile-undersaturated conditions) volatiles may stall at the interface between the two magmas because they do not achieve the residual saturation threshold (i.e., lack of gas permeability). Under these conditions volatiles prevent defrosting of the mush and cooling of the mafic body as heat transfer is impeded (i.e., "thermos bottle effect"; Carrigan 1988; Koyaguchi and Kaneko 1999; 2000; Huber et

Always consult and cite the final, published document. See http:/www.minsocam.org or GeoscienceWorld

al. 2009; 2010). When heat advection by volatile flux following multiple mafic pulses intruding into a felsic crystal mush is efficient, it may trigger mush rejuvenation and/or melt extraction.

Insights into mafic-felsic magma interactions are provided by numerous field examples (e.g., Poldervaart and Taubeneck 1959; Loomis 1963; Moore and Lockwood 1973; Shannon et al. 1982; D'Lemos 1987; Frost and Mahood 1987; Gourgaud and Villemant 1992; Seaman and Ramsey 1992; Sisson et al. 1996; Humphreys et al. 2010). A well-known example is the Tertiary Adamello Massif (Italy), a batholith characterised by tonalite and subordinate granodiorite plutons associated with small mafic/ultramafic intrusions, syn-plutonic mafic dykes and sills, and ubiquitous mafic inclusions (Blundy and Sparks 1992; John and Blundy 1993; Broderick et al. 2015; Hürlimann et al. 2016). Mixing textures between tonalite and mafic magmas are apparent in the field. The mafic bodies are texturally and compositionally heterogeneous as a result of variable assimilation of tonalite leading to xenocrystic textures. For example, reaction of quartz phenocrysts from the tonalite with fine-grained, dark, hornblende-bearing mafic magma produces coronas of green hornblende (Figure 1). The presence of hornblende in the gabbroic rock suggests significant H_2O in the hot (1050 °C) mafic melt (≥ 4 wt% H_2O; e.g. Yoder and Tilley 1962; Holloway and Burnham 1972), which ascended rapidly from the deep crust (7 kbar; Ulmer 1988; 2007; Ulmer et al. 1983) and interacted with hot (850 °C), partially molten tonalite (Figure 1). Disaggregation and swarms of mafic inclusions, schlieren and sub-parallel sheets of fine-grained mafic material, intimately mingled with the crystal-rich tonalite. In the light of such observations, the tonalite body evidently was in a mushy state, and could be mobilised with sufficient ease to allow partial hybridisation (Blundy and Sparks 1992). Mobilisation was made possible by the

Always consult and cite the final, published document. See http:/www.minsocam.org or GeoscienceWorld

transfer of heat to the tonalite from the cooling mafic magma. Diffusion and/or exsolution of volatiles from the mafic sheets, as evinced by the ubiquitous gabbroic pegmatites, would have facilitated host rock mobilisation. Throughout the Adamello batholith, but most notably in the southern part, hydrous mafic magmas intrude felsic host magmas, supplying heat and volatiles that can be seen to contribute to the physical destabilisation and extraction of melts from the host (Ulmer et al. 1983; Blundy and Sparks 1992). Particularly, field observations of the leucogranite dikes extending radially out from the Listino Ring Complex are suggestive of residual melt that was expelled from Monoccola Granodiorite after the emplacement of the hydrous Listino Ring Gabbro (John and Blundy 1993). The rapid cooling and crystallisation of this gabbro led to volatile exsolution and consequent volume expansion of the overlying mush, resulting in roof uplift and the formation of inward dipping shear fractures on the shoulders of the melt-mush system. At the same time, the release of heat and volatiles caused partial melting and remobilisation of the Monoccola Granodiorite mush and consequent melt extraction as confirmed by the leucogranite dikes of the Listino Ring Complex, with an extracted melt volume of ~10-22 vol%, in agreement with field observations (Verberne et al. 2011).

To simulate the chemical and physical conditions of crystal mush rejuvenation and test melt extraction induced by hot, H_2O-rich mafic intrusions, we conducted experiments on a suite of H_2O-undersaturated (4 wt% H_2O in the interstitial melt) quartz-bearing dacite crystal mushes (crystal fraction, ϕ = 0.5-0.8) subject to volatile supply from an H_2O-saturated (≥ 6 wt% H_2O), crystal-free andesite at 4 kbar and 950 °C, in a closed-system (i.e., no net loss of volatiles). We applied an experimental setup already used in previous works (Yoder 1973; Johnston and Wyllie 1988; van der Laan and Wyllie 1993), but imposing an initial water gradient between andesite and

Always consult and cite the final, published document. See http:/www.minsocam.org or GeoscienceWorld

dacite (Pistone et al. 2016). The isothermal nature of the experiments simulates the situation where intruding mafic magma (at ~1050 °C) and host tonalite (at ~850 °C) have equilibrated thermally at the interface (i.e., the temperature within the experimental system is spatially and temporally uniform) following heat diffusion and prior to chemical interaction. This situation is consistent with the more rapid diffusion of heat compared to most chemical components, including H_2O (i.e. thermal diffusivities are of the order of 10^{-7} m^2/s in H_2O-bearing rhyolitic melts at > 800 °C; Romine et al. 2012; the diffusivity of H_2O is about 10^{-10} m^2/s in hydrous rhyolite at 950 °C and 4 kbar [experimental conditions of this study]; Ni and Zhang 2008). The two systems are characterised by different liquidus temperatures (816 °C in the andesite and 923 to 1109 °C in the dacite, depending on the crystal content; Pistone et al. 2016), which are mainly dictated by the initial H_2O contents in each end-member. The subsequent change of liquidi in both systems, with the andesite liquidus rising and the dacite liquidus decreasing, is caused by the H_2O diffusion from the andesite to the dacite during experiments (Pistone et al. 2016). At the conditions of the experiment the H_2O content of the felsic crystal mush is limited by the H_2O stored in the interstitial melt phase, thus the *bulk* mush is always H_2O-undersaturated. Once it is heated the melting phase relations, in the absence of added H_2O, will be characterised by water activity (aH_2O) less than one. This limits the amount of melt production that can occur by heating alone. This situation prevails even when the interstitial melt phase is H_2O-saturated. The H_2O-undersaturated nature of the bulk felsic crystal mush therefore simulates the condition of a mush that experienced thermally-induced, dehydration partial melting rendering the melt undersaturated by the time that diffusive addition of H_2O starts to play a role. Then, the crystallinity of the felsic mush reflects different degrees of melting of the original mush after the release of the

Always consult and cite the final, published document. See http:/www.minsocam.org or GeoscienceWorld

heat by the intruding mafic magma. The mafic end-member is initially crystal-free consistent with rapid ascent to shallow depth without crystallising en route. The equilibration pressure is ~4 kbar (minimum pressure in a conventional piston cylinder), comparable to that in the Adamello Massif (2-3 kbar). The run products reported here are those presented by Pistone et al. (2016), who mainly focussed on the kinetics of nucleation and crystallisation and consequent formation of unidirectional solidification textures or comb layering in mafic enclaves. Here we concentrate on selected run products to show the H_2O diffusion from crystallising mafic magmas and how this enhances further partial melting of the felsic mushes, physical changes in the residual melt phase (i.e., density and viscosity) and, potentially, melt extraction after heat and H_2O diffusion.

Experimental methodology

Sample preparation and synthesis procedures are described in detail in Pistone et al. (2016). Cylindrical samples (3 mm diameter and length ranging from 1.2 to 3.6 mm) of synthetic hydrous dacite crystal mush, with different fractions of quartz particles (F50: $\phi = 0.5$; F60: $\phi = 0.6$; F70: $\phi = 0.7$; F80: $\phi = 0.8$; H_2O ranging from 2.1 wt.% in the least crystalline sample to 0.84 wt.% at the highest crystallinity), were juxtaposed with hydrous ($\geq$ 6 wt% H_2O) crystal-free andesite glass. To ensure a perfect initial contact between the interacting samples, the synthesised glasses were polished on the top and bottom surfaces, and inserted in welded Au capsules (3-4 mm diameter), which, in turn, were inserted in larger Mo-lined Au capsules (6 mm diameter) filled with Al_2O_3 powder and deionised H_2O (0.1-0.2 ml). Two different interaction setups were used: i) classic two-layer Setup A with felsic overlying mafic, and ii) "intrusion-type" Setup B with mafic sandwiched between felsic samples. The

Always consult and cite the final, published document. See http:/www.minsocam.org or GeoscienceWorld

two approaches allowed simulation of mafic-felsic magma interaction at different mass ratios (mafic-felsic ratio of ~1:1 in Setup A, and ~1:2 in Setup B). Experiments were carried out in an end-loaded Boyd and England (1960)-type piston cylinder apparatus using a 19 mm talc-pyrex, tapered-furnace cell (McDade et al 2002). Calibrations (based on water solubility in silicic melts) suggest a 20% lower value than the 5 kbar calculated from the hydraulic oil pressure on the piston. As a result our sample pressure is believed to be in the range 4 to 4.5 kbar. Temperature was monitored by a D-type ($W_{97}Re_3/W_{75}Re_{25}$) thermocouple connected to a Eurotherm 800 series controller, with no correction for the pressure effect on the emf (Mao and Bell 1971). The hot piston-out technique (Johannes et al. 1971) was used in all experiments. The intrinsic fO_2 of this assembly is relatively oxidised (NNO+1 to +2). As a result of the reduced conditions used for preparation of the starting material (~NNO-4), the oxidising external environment might encourage H_2 to diffuse out of the sample capsule with a simultaneous conversion of Fe^{2+} to Fe^{3+}. However, our use of Au inner and Mo-lined outer Au capsules was designed to minimise H_2 loss; there was no obvious loss of H_2O at the sample edge and certainly not in the centre of the experiment where we report our data. Experiments ran for 24 hours and were terminated by turning off the power. Recovered charges were impregnated in epoxy and polished prior to analytical inspections.

Analytical techniques

EPMA, FEG-EPMA, and SEM

Glass and mineral compositions from the starting materials and experimental charges were analysed with a conventional, tungsten-sourced 5-WD spectrometer CAMECA SX-100 wavelength-dispersive electron probe micro-analyser (EPMA).

Always consult and cite the final, published document. See http:/www.minsocam.org or GeoscienceWorld

Glass compositions were investigated with a 15 kV accelerating voltage, 2-5 nA beam current and 10-20 μm diameter (defocused) beam, and a counting time of 20 s (peak) and 10 s (background). Minerals were analysed with a focused (1 μm) 10 nA beam current and 20 kV accelerating voltage. Natural and synthetic standards were employed and data were ZAF corrected. Peak count times of 60 s for Ca, Al, Ti, Fe and Mg, 30 s for Si, K, and 20 s for Na. Spectrometers were set to analyse K, Na and Si first. Primary calibrations used a mixture of synthetic and natural standards and secondary standards of Kakanui kaersutite KK1 (Jarosewich et al. 1980), natural diopside, USGS basaltic glass reference BCR2-G (Govindaraju 1994) and hydrous dacite glass F0 (Pistone et al. 2016). Glass and mineral compositions are reported by Pistone et al. (2016).

Using the approach of Saunders et al. (2014) to analyse crystal zoning, lines of high-spatial resolution spot analyses through quartz crystals and surrounding glass in representative run product F70-M were conducted using a JEOL 8530F field emission gun electron probe micro-analyser (FEG-EPMA). Analyses were carried out with a 10 kV acceleration voltage, 1 nA beam current, and 1 μm beam diameter. Primary calibrations for FEG-EPMA used the same primary and secondary standards as conventional EPMA. FEG-EPMA data are reported in Supplementary Materials.

Backscattered (BSE) images of run products were acquired with a Hitachi S-3500N quad solid-state BS detector scanning electron microscope (SEM). An accelerating voltage of 15 to 25 kV and a beam current of 1 nA were employed to obtain good contrast between glass and minerals. Images were used to estimate volume fraction and size of the different phases in different portions of the run products using JMicro-Vision v1.2.7.

Always consult and cite the final, published document. See http:/www.minsocam.org or GeoscienceWorld

SIMS

Glassed starting materials and run products were analysed by secondary ion mass spectrometry (SIMS) for dissolved H_2O using a CAMECA ims-4f ion microprobe at the EIMF of the University of Edinburgh. Au-coated samples were analysed with a 1.5 nA, 10.8 kV $^{16}O^-$ beam focussed to a 10 μm spot, with ~15 keV net impact energy. Positive secondary ions were extracted at 4.5 keV with a 75±40 eV offset to minimise molecular ion transmission. Prior to each analysis, a 7 μm^2 raster was applied for 2 minutes at the target glass areas to remove any surface contamination around the edge of the sputter pit. NIST-610 (Hinton 1999) and natural and synthetic hydrous silica-rich glasses (including the crystal-free felsic and mafic compositions) were used as standards to monitor the H/Si ion yield and background at the start of each day. The number of counted cycles was 10, corresponding to a counting time of about 10 minutes. In addition to ^{1}H and ^{30}Si, ^{7}Li, ^{11}B, ^{26}Mg, ^{42}Ca, ^{47}Ti, and ^{54}Fe were measured, with the heavier elements used to assess consistency with major element compositions from EPMA. The background H_2O correction measured on NIST-610 was equivalent to ≤ 0.2 wt% H_2O. The analytical data, Si-normalised and corrected using the NIST-610 standard of the GeoReM database (http://georem.mpch-mainz.gwdg.de/), are reported in Pistone et al. (2016).

Raman spectroscopy

Raman-based spectra and OH-intensity maps of the run products were performed using a Thermo Scientific™ DXR™ confocal Micro-Raman spectrometer (grating of 1800 mm^{-1}) equipped with an Olympus microscope and an Ar-ion laser (wavelength of 514.5 nm). Reflected light optics was used to select analysis locations. Raman spectra for H_2O determination were acquired for 120 s in the range of 200-

Always consult and cite the final, published document. See http:/www.minsocam.org or GeoscienceWorld

1500 and 2800-3850 cm^{-1} encompassing low- and high-frequency vibrational bands associated with the silicate glass network and vibration modes of OH and H_2O, respectively, at room conditions (25 °C and 1 bar). The Raman optics and precision-control stage give lateral and vertical resolution of 250 nm and 500 nm, respectively, and were used in rapid spectra acquisition mode (less than 100 ms for a single spectrum). The effective volume resolution was better than 5 μm^3. Maps were obtained in confocal mode and spectra (120 s each) were obtained from a grid of points spaced 2 µm apart, at a constant sample depth of 5±2 µm. Although the objective was to map gradients, some quantification of H_2O contents was attempted using the Raman spectra and a set of well-characterised hydrous rhyolite and andesite glass standards with known H_2O contents determined by SIMS at the University of Edinburgh and Karl-Fischer titration at ETH-Zürich (Pistone et al. 2015). The calibration followed the method of Le Losq et al. (2012) relating the peak ratios of the low-frequency peak (at 1128 ±5 cm^{-1}) to the OH/H_2O peak (at 3568 ±10 cm^{-1}).

Results

Run products are labelled with the abbreviations of the two or three separate components loaded and labelled in the following way; e.g., M-F50 is a couple made of mafic andesite (M), which is always crystal-free, and felsic dacite (F) that has a specified initial crystal fraction (ϕ) of 0.5 (F50); e.g. F60-M-F60 is a sandwich of andesite between two layers of crystal-bearing ($\phi = 0.6$) dacite, etc.

Microstructures

All run products are characterised by extensive crystallisation of the andesite sample, which becomes more evident when Setup B (F-M-F sandwich) is used

Always consult and cite the final, published document. See http:/www.minsocam.org or GeoscienceWorld

(Figure 2B). The andesite shows a decrease of the local glass fraction by ~0.7 to ~0.95 towards the interface. Conversely, the dacite crystal mushes are characterised by the presence of a thin (30 to 60 μm thick) portion of crystal-free glass (with rare vesicles) close to the interface with the andesite sample (see image inset in Figure 2A). Moving further from the interface, this layer is followed by another relatively thin (~150-200 μm) region of nuclei and microlites of hornblende (accompanied by a few isolated vesicles), which are mostly located close to the quartz crystal clusters (see image inset in Figure 2A). Quartz crystals, which make up the solid framework of the felsic mushes, display smooth boundaries (Figure 2D) and, in some places, are surrounded by 1-3 μm-sized hornblende microlites (see image inset in Figure 2A). More importantly, it is possible to observe that the dacite mushes with $\phi < 0.8$ are affected by large textural heterogeneities at several hundreds μm- to mm-scale, characterised by large crystal-free glass pools, whose areas decrease with increasing crystallinity (Figure 2A-C). At $\phi = 0.8$, there is lack of glass-enriched portions generated during interaction experiments (see Pistone et al. 2016).

Chemistry

One of the major chemical changes observed in the glass of the felsic mushes following interaction is an increase in SiO_2 content above that of the starting glass. This is particularly evident where the glass is surrounded by quartz crystals, suggestive of quartz dissolution, as confirmed by FEG-EPMA analysis (Figure 2D). More details on chemical mixing in the run products are reported in the study of Pistone et al. (2016). Here we focus attention on the variation of H_2O.

At the end of the run H_2O contents in the glass (Figure 2) increase from the dacite (5-6 wt% H_2O) to the andesite (7-8 wt%), consistent with a flux of H_2O from

Always consult and cite the final, published document. See http:/www.minsocam.org or GeoscienceWorld

the latter to the former. In the dacite H_2O contents are high in proximity to the interface, particularly in the glass-rich regions, but relatively close to the initial H_2O content in glass pockets within or surrounded by quartz crystal clusters and in the glassy portions more than 0.2 mm from the interface (Figure 2A-C). Bulk H_2O contents change dramatically from the andesite to the dacite, particularly along the interface (< 1 mm distance from the interface; Figure 3) where the andesite is largely crystalline (ϕ > 0.9), but the dacite is glassy or displays limited hornblende crystallisation (ϕ < 0.07) around quartz crystals (see image inset in Figure 2A). Bulk H_2O contents (i.e. accounting for the presence of crystals) vary from < 0.8 wt% in the upper portion of the andesite (< 1 mm from the interface) to 1-3 wt% in the dacite. We observe that, overall, the greater the crystal content in the dacite mush, the higher the H_2O content in the glass and the lower the H_2O content in the bulk dacite (Figure 3) suggestive of local H_2O solubility increase as the residual melt becomes enriched in SiO_2 through quartz dissolution (Figure 2D). The run product F80-M-F80 (Figure 3D) represents an exception since both H_2O contents in the glass (3-4 wt%) and in the bulk dacite (0.4-0.6 wt%) are lower than H_2O contents in the other run products (Figure 3), suggestive of a combination of large crystal content in the mush and dissolution of quartz in the residual melt. These results demonstrate how the interplay between crystallisation (reducing bulk H_2O storage capacity) and melting (increasing storage capacity) mediates the flux of H_2O from the andesite to the dacite. The implications of these coupled processes for natural mixed-magma settings is discussed below.

Discussion

Melt dehydration during isothermal decompression is a widespread cause of crystallisation in hydrous magmas due to the strong effect of H_2O on liquidus

Always consult and cite the final, published document. See http:/www.minsocam.org or GeoscienceWorld

temperatures and phase relations (Yoder et al. 1957; Tuttle and Bowen 1958; Burnham and Jahns 1962; Merrill and Wyllie 1975; Blundy and Cashman 2001). Thus, we expect that volatile exsolution, outgassing, and diffusion, including changes in H_2O pressure, that occur during interactions between hydrous magmas in the crust might also have significant consequences for phase relations, notably by maintaining high aH_2O in the felsic mush.

The experiments show that isothermal interaction of mafic and felsic magmas produces complex relationships. The interaction (or contact) temperature (controlled by heat transfer) and liquidus temperature (controlled by volatile transfer) of each domain determines: i) undercooling-driven crystallisation when contact temperature < liquidus temperature, or ii) superheating-driven melting when contact temperature > liquidus temperature. In the case of isothermal interaction, changes in liquidus temperature are driven by the movement of water from one magma to the other. Undercooling driven by water loss is termed "chemical undercooling" by Pistone et al. (2016). The textures that result from undercooling depend on its magnitude: large values of undercooling favour crystal nucleation, while small values of undercooling favour crystal growth (e.g., Brandeis and Jaupart 1987; Cashman and Blundy 2000; Hort 1998). For chemical undercooling, it is the rate of loss of H_2O that determines the texture. A front of increasing liquidus temperature, due to H_2O loss and consequent crystallisation, will propagate into the mafic domain (i.e., inward solidification front driven by volatile release; Podlachikov and Wickham, 1994), as H_2O moves to the felsic domain (Figures 2-3). Depending on the evolution of undercooling with time the migration of the crystallisation front may be dominated either by nucleation or growth (Pistone et al. 2016). In natural hydrous magmas the chemical (H_2O-driven) and thermal (temperature-driven) "undercooling fronts"

Always consult and cite the final, published document. See http:/www.minsocam.org or GeoscienceWorld

propagate away from the interface at rates controlled by the relative diffusivities of H_2O and heat. Although heat diffuses three orders of magnitude faster than H_2O, the effect of reducing the temperature on undercooling is much less pronounced than the effect of dehydration on raising the liquidus temperature in the mafic magma. The corollary occurs in the felsic domain, where both heat and H_2O are being supplied, leading to "chemical superheating" as the liquidus temperature is reduced by H_2O addition. The addition of H_2O maintains aH_2O at or close to one in the mush, thereby enabling higher degrees of melting than would be possible if bulk mush H_2O content was limited by that originally contained in the residual melt phase.

In the light of field observations and rock textures explored in the natural samples from the Val Fredda Complex in the Tertiary Adamello Batholith (Alps, Italy) (Figure 1), and the petrological constraints reported in previous works (Blundy and Sparks 1992; John and Blundy 1993; Ulmer 1988; 2007; Ulmer et al. 1983; Broderick et al. 2015; Hürlimann et al. 2016), here we attempt to evaluate the independent effects of heat and H_2O addition to a felsic system destabilised by a mafic intrusion. We underline that the design of our experiments did not capture the effect of heat diffusion during magma mixing. In a natural scenario the fast transfer of heat from the intruding water-rich mafic to the water-saturated felsic magma (i.e. crystals plus H_2O-bearing interstitial melt) dictates a temperature convergence for both systems, due to which the mafic magma cools and initiates to crystallise as a consequence of heat loss, whereas the felsic host is reheated and experiences partial melting (Figure 4A). The felsic partial melting can affect a number of minerals such as quartz, feldspar, biotite, amphibole; particularly, the melting of anhydrous phases, such as the quartz particles used in our experiments, induces the felsic system to become water-undersaturated (Figure 4A). This condition drives a flux of H_2O from

Always consult and cite the final, published document. See http:/www.minsocam.org or GeoscienceWorld

the cooling volatile-rich mafic intrusion. Therefore, the melting of anhydrous phases triggers more melting by "absorbing" water under isothermal conditions. The addition of water suppresses the felsic liquidus temperature (Figure 4B), down to as much as 800 °C (Pistone et al. 2016). Concomitantly, the mafic magma dehydrates and is fated to quench chemically against the felsic system, leading eventually to complete solidification and "viscous death" (Annen et al. 2006; Pistone et al. 2013). In such a context, the overall felsic mush rejuvenation process consists of two main stages: i) an "early rejuvenation stage" in which the partial melting of the felsic host is heat-driven (Figure 4A); and ii) a "mature rejuvenation stage" in which the partial melting of the felsic system is water-driven (Figure 4B). In detail, the final equilibration temperature depends on the heat contents of the mafic and felsic systems at the scale on which interaction occurs. In nature, masses and volumes of igneous bodies are extremely difficult to estimate in the field since erosion and tectonic processes tend to obscure such information. In the case of Adamello, the intruding mafic magmas consist of dykes and swarms of inclusions that make it even more difficult assess the effective mass and volume of the intruding mafic magmas.

Implications

Petrological and numerical studies have proposed that rejuvenation might generate active magma chambers in the Earth's crust (e.g., Bachmann and Bergantz 2003; Bain et al. 2013). Silicic magma bodies composed of a touching framework of crystals and interstitial melt, close to their rheological lockup point, are remobilised in response to the injection of hotter, hydrous mafic magma providing mass, heat and volatiles (Eichelberger 1995; Bachmann and Bergantz 2003; Huber et al. 2009; Parmigiani et al. 2014). As shown in Figure 4, heat and volatile transfer from a

Always consult and cite the final, published document. See http:/www.minsocam.org or GeoscienceWorld

crystallising layer of injected mafic magma, ponded at the floor of a silicic pluton or magma body, can melt, weaken, and destroy the crystalline framework of the underlying silicic mush, rendering it gravitational unstable (e.g., Jellinek and Kerr 1999; Bain et al. 2013). When the crystalline framework is not fully destroyed, and, thus, the felsic crystal mush remains partially molten, the rejuvenation process might not favour the mobilisation of the whole mush, but can drive the extraction of interstitial melts from the mush, potentially generating caps or lenses of evolved, crystal-poor melts (e.g., Hildreth and Wilson 2007; Czuppon et al. 2012). In the light of our experiments simulating the water-driven "mature rejuvenation stage" of felsic systems (Figure 4B), we propose to test whether water diffusion promotes not only enhanced melt production, but also melt extraction from the mush. Specifically, we quantify the decrease in density (ρ_{melt}) and viscosity (η_{melt}) of silicic melt affected by the flux of H_2O via diffusion, and understand how these physical changes assist melt extraction from the mush. Figures 5 and 6 show ρ_{melt} and η_{melt} profiles of the residual melt in both dacite and andesite. ρ_{melt} and η_{melt} were calculated using the models of Lange and Carmichael (1987) and Giordano et al. (2008), respectively, under our experimental conditions of temperature and pressure, and using the analytical data from Pistone et al. (2016). The density model of Lange and Carmichael (1987) was combined with the densification model of Ardia et al. (2014), who propose a linear increase of ρ_{melt} at P < 15 kbar. The 1 bar-based viscosity model of Giordano et al. (2008) was modified using a correction factor of 1.8 log units in η_{melt} to include the pressure effect on the viscosity of polymerised melts, with η_{melt} decreasing with pressure under the conditions of > 800 °C and < 15 kbar (Ardia et al. 2008; 2014; Pistone et al. 2012). In our interaction experiments ρ_{melt} values are higher in the andesite (2250-2450 kg/m^3; Figure 5) than in the dacite (2050-2150 kg/m^3; Figure 5).

Always consult and cite the final, published document. See http:/www.minsocam.org or GeoscienceWorld

In some dacite portions where quartz crystals isolate melt pockets, the inferred ρ_{melt} is slightly higher (2200-2250 kg/m^3). η_{melt} tends to increase by 1 log unit from andesite to dacite (Figure 6). Only in run product F80-M-F80 η_{melt} of andesite is higher than that of dacite (Figure 6). The increase of both ρ_{melt} and η_{melt} in the andesite and their decrease in the dacite are consistent with andesite dehydration and dacite hydration respectively.

The simultaneous decrease of ρ_{melt} and η_{melt} in the felsic melts may lead to the extraction of the residual silicic melt from the mush. In nature, in the absence of other processes such as gas-driven filter pressing (Anderson et al. 1984; Sisson and Bacon 1999; Pistone et al. 2015), to be effective, melt extraction must occur within the lifetime of crystal mushes in the Earth's crust (average 10^4-10^5 years; Bachmann and Bergantz 2004, and references therein; 10^7 years for assembled plutons; Glazner et al. 2004). Using a simple approximation of the H_2O diffusion length scale ($x = \sqrt{t \times D_{H_2O}}$, Watson 1982; Baker 1991; with $D_{H_2O} = 3 \cdot 10^{-10}$ m^2/s from Ni and Zhang 2008, and t = experimental duration), in our experiments H_2O penetrates the whole felsic sample (x = 5.4 mm) within 24 hours and drives lower ρ_{melt} and η_{melt} as well as ρ_{bulk} and η_{bulk} (Figures 5-6). However, in natural systems at the scale of tens of meters to kilometre scale, H_2O diffusion is not sufficient to stimulate melt extraction within the lifetime of felsic plutons in the Earth's crust, including those of high longevity such as the Tuolumne Intrusive Suite, Yosemite Valley (~10 My; Glazner et al. 2004; Figure 7).

In conclusion, we investigated experimentally H_2O transfer during high-temperature and -pressure mixing between H_2O-undersaturated dacite crystal mush and H_2O-saturated andesite magma at crustal conditions (950 °C, 4 kbar) under conditions that heat transfer had already occurred. The microstructural and chemical

Always consult and cite the final, published document. See http:/www.minsocam.org or GeoscienceWorld

results for the run products show that isothermal undercooling results from a change in liquidus temperatures of the interacting magmas with changing H_2O content. Mafic samples crystallised at the same time as H_2O diffusion into the felsic end-members, which became enriched in H_2O, generating partial melting of the crystal network (i.e., quartz dissolution) and inducing changes in the physical properties (i.e., density and viscosity) of the residual melt. Mixing between pulses of hot and H_2O-saturated mafic magma and near-solidus felsic crystal mushes in the Earth's crust are important instances of heat and volatile transfer to the felsic system that may promote crystal mush rejuvenation (through progressive reheating and partial melting). The heat-driven rejuvenation stage first and, then, the water-driven melting of the felsic mush may lead to a consequent extraction of the residual melt from the mush. In the latter stage of the rejuvenation process, large addition of water into felsic magmas, which became H_2O-undersaturated during partial melting of anhydrous phases due to heat transfer, may reactivate "old" magma chambers (e.g., Dolfi and Trigila 1978) or generate new ones (i.e., formation of "ghost" magma chambers; Trigila et al. 2008) by decreasing liquidus temperature. This process of rejuvenation differs significantly from that driven solely by the transfer of heat, because of the enhanced melt productivity in the mush due to H_2O addition. However, using existing models for testing melt extraction from mushes in a scenario similar to that experimentally tested, water diffusion alone is not sufficient to drive melt extraction from a mush within the lifetime of crustal felsic plutons. As reported in previous studies modelling melt extraction from felsic mushes after being intruded by mafic intrusions (e.g., Bachmann and Bergantz 2004; 2006; Huber et al. 2009; 2010; 2011; Parmigiani et al. 2014), exsolved volatiles (i.e., gas bubbles) might play an essential role in favouring rapid melt extraction from felsic plutons. To our knowledge, there are no

Always consult and cite the final, published document. See http:/www.minsocam.org or GeoscienceWorld

experimental constraints that can support the numerical results of the existing models; future investigations could assess how the mechanics and mechanisms of exsolved volatile transfer during magma mixing events might favour efficient melt extraction from felsic mushes.

Acknowledgments

SNSF Grant EPM-PBEZP2_14922 (to MP), and ERC Advanced Grant CRITMAG, NERC SIMS award IMF534/0514 and a Wolfson Research Merit Award (to JB) supported this research. We acknowledge the following for their help: S. Kearns and B. Buse for EPMA, FEG-EPMA, and SEM analyses (University of Bristol); R. Hinton for SIMS analyses (EIMF, University of Edinburgh); C. Clapham and D. Hawley for technical support (University of Bristol); J. Riker (University of Bristol) for providing hydrous glass standards for SIMS; Alberto Luisoni AG (Switzerland) and Nabaltec AG (Germany) for supplying quartz and APYRAL 60CD used in the starting materials; M. Petrelli, C. Huber, and an anonymous reviewer for their helpful comments on an earlier version of the manuscript.

References

Anderson, A.T. Jr., Swihart, G.H., Artioli, G., and Geiger, C.A. (1984) Segregation vesicles, gas filter-pressing, and igneous differentiation. Journal of Geology, 92, 55-72.

Annen, C., Blundy, J.D., and Sparks, R.S.J. (2006) The genesis of intermediate and silicic magmas in deep crustal hot zones. Journal of Petrology, 47, 505-539.

Ardia, P., Giordano, D., and Schmidt, M.W. (2008) A model for the viscosity of rhyolite as a function of H_2O-content and pressure: a calibration based on centrifuge piston cylinder experiments. Geochimica et Cosmochimica Acta, 72, 6013-6123.

Always consult and cite the final, published document. See http:/www.minsocam.org or GeoscienceWorld

Ardia, P., Di Muro, A., Giordano, D., Massare, D., Sanchez-Valle, C., and Schmidt, M.W. (2014) Densification mechanisms of haplogranite glasses as a function of water content and pressure based on density and Raman data. Geochimica et Cosmochimica Acta, 138, 158-180.

Bachmann, O., and Bergantz, G.W. (2003) Rejuvenation of the Fish Canyon magma body: a window into the evolution of large-volume silicic magma systems. Geology, 31, 789-792.

Bachmann, O., and Bergantz, G.W. (2004) On the origin of crystal-poor rhyolites: extracted from batholitic crystal mushes. Journal of Petrology, 45, 1565-1582.

Bachmann, O., and Bergantz, G.W. (2006) Gas percolation in upper-crustal silicic crystal mushes as a mechanism for upward heat advection and rejuvenation of near-solidus magma bodies. Journal of Volcanology and Geothermal Research, 149, 85-102.

Bain, A.A., Jellinek, A.M., and Wiebe, R.A. (2013) Quantitative field constraints on the dynamics of silicic magma chamber rejuvenation and overturn. Contributions to Mineralogy and Petrology, 165, 1275-1294.

Baker, D.R. (1991) Interdiffusion of hydrous dacitic and rhyolitic melts and the efficacy of rhyolite contamination of dacitic enclaves. Contributions to Mineralogy and Petrology, 106, 462-473.

Barboza, S.A., and Bergantz, G.W. (1997) Melt productivity and rheology: complementary influences on the progress of melting. Numerical Heat transfer, Part A: Applications, 31, 475-492.

Blundy, J.D., and Sparks, R.S.J. (1992) Petrogenesis of mafic inclusions in granitoids of the Adamello Massif, Italy. Journal of Petrology, 33, 1039-1104.

Blundy, J.D., and Cashman, K.V. (2001) Magma ascent and crystallization at Mount St. Helens, 1980-1986. Contributions to Mineralogy and Petrology, 140, 631-650.

Blundy, J.D., Cashman, K.V., Rust, A., and Witham, F. (2010) A case for CO_2-rich arc magmas. Earth and Planetary Science Letters, 290, 289-301.

Bohrson, W.A., and Spera, F.J. (2001) Energy-constrained open system magmatic processes II: Application of energy-constrained assimilation–fractional crystallization (EC-AFC) model to magmatic systems. Journal of Petrology, 42, 1019-1041.

Boyd, F.R., and England J.L. (1960) Apparatus for phase equilibrium measurements at pressures of up to 50 kbars and temperatures to 1750 ºC. Jorunal of Geophysical Research, 65, 741-748.

Brandeis, G., and Jaupart, C. (1987) The kinetics of nucleation and crystal growth and scaling laws for magmatic crystallization. Contributions to Mineralogy and Petrology, 96, 24-34.

Always consult and cite the final, published document. See http:/www.minsocam.org or GeoscienceWorld

Broderick, C., Wotzlaw, J.F., Frick, D.A., Gerdes, A., Ulianov, A., Günther, D., and Schaltegger, U. (2015) Linking the thermal evolution and emplacement history of an upper-crustal pluton to its lower-crustal roots using zircon geochronology and geochemistry (southern Adamello batholith, N. Italy). Contributions to Mineralogy and Petrology, 170, 28-44.

Burgisser, A., and Bergantz, G.W. (2011) A rapid mechanism to remobilize and homogenize crystalline magma bodies. Nature, 471, 212-215.

Burnham, C.W., and Jahns, R.H. (1962) A method for determining the solubility of water in silicate melts. American Journal of Science, 260, 721-745.

Caricchi, L., Burlini, L., Ulmer, P., Gerya, T., Vassalli, M., and Papale, P. (2007) Non-Newtonian rheology of crystal-bearing magmas and implications for magma ascent dynamics. Earth and Planetary Science Letters, 264, 402-419.

Caricchi, L., and Blundy, J.D. (2015) The temporal evolution of chemical and physical properties of magmatic systems. In Caricchi, L., and Blundy, J.D. (eds) Chemical, Physical and Temporal Evolution of Magmatic Systems. Geological Society of London, Special Publication, 422, http://doi.org/10.1144/SP422.11.

Carrigan, C.R. (1988) Biot number and thermos bottle effect: implications for magma chamber convection. Geology, 16, 771-774.

Cashman, K.V., and Blundy, J.D. (2000) Degassing and crystallization of ascending andesite and dacite. Philosophical Transactions of the Royal Society A, 358, 1489-1513.

Cervantes, P., and Wallace, P. (2003) Role of H_2O in subduction-zone magmatism: newinsights from melt inclusions in high-Mg basalts from central Mexico. Geology, 31, 235-238.

Chiaradia, M., Müntener, O., and Beate, B. (2011) Enriched basaltic andesites from mid-crustal fractional crystallization, recharge, and assimilation (Pilavo Volcano, Western Cordillera of Ecuador). Journal of Petrology, 52, 1107-1141.

Czuppon, G., Lukacs, R., Harangi, S., Mason, P.R.D., and Ntaflos, T. (2012) Mixing of crystal mushes and melts in the genesis of the Bogacs ignimbrite suite, northern Hungary; an integrated geochemical investigation of mineral phases and glasses. Lithos, 148, 71-85.

D'Lemos, R.S. (1987) Relantionships between the Cobo Granite and the Bordeaux Diorite Complex, Guernsey. PhD Dissertation, University of Bristol.

Dolfi, D., and Trigila, R. (1978) The role of water in the 1944 Vesuvius Eruption. Contributions to

Always consult and cite the final, published document. See http:/www.minsocam.org or GeoscienceWorld

Mineralogy and Petrology, 67, 297-304.

Dufek, J., and Bergantz, G.W. (2005) Lower crustal magma genesis and preservation: A stochastic framework for the evaluation of basalt-crust interaction. Journal of Petrology, 46, 2167-2195.

Dungan, M.A., and Davidson, J. (2004) Partial assimilative recycling of the plutonic roots of arc volcanoes: an example from the Chilean Andes. Geology, 32, 773-776.

Eichelberger, J.C. (1995) Silicic Volcanism: ascent of viscous magmas from crustal reservoirs. Annual Reviews of Earth and Planetary Science, 23, 41-63.

Eichelberger, J.C., and Izbekov, P.E. (2000) Eruption of andesite triggered by dyke injection: contrasting cases at Karymsky Volcano, Kamchatka and Mt Katmai, Alaska. Philosophical Transactions of the Royal Society A, 358, doi:10.1098/rsta.2000.0599.

Frost, T.P., and Mahood, G.A. (1987) Field, chemical, and physical constraints on mafic-felsic magma interaction in the Lamarck Granodiorite, Sierra Nevada, California. Geological Society of American Bulletin, 99, 272-291.

Giordano, D., Russell, J.K., and Dingwell, D.B. (2008) Viscosity of magmatic liquids: a model, Earth and Planetary Science Letters, 271, 123-134.

Glazner, A.F., Bartley, J.M., Coleman, D.S., Gray, W., and Taylor, R.Z. (2004) Are plutons assembled over millions of years by amalgamation from small magma chambers?. Geological Society of America Today, 14, 4-11.

Govindaraju, K., (1994) 1994 compilation of working values and sample description for 383 geostandards. Geostandards Newsletter, 18, 1-158.

Gourgaud, A., and Villemant, B. (1992) Evolution of magma mixing in an alkaline suite: the Grande Cascade sequence (Monts-Dore, French Massif Central). Geochemical modeling. Journal of Volcanology and Geothermal Research, 52, 255-275.

Hildreth, W., and Moorbath, S. (1988) Crustal contributions to arc magmatism in the Andes of Central Chile. Contributions to Mineralogy and Petrology, 98, 455-489.

Hildreth, W., and Wilson, J.N. (2007) Compositional Zoning of the Bishop Tuff. Journal of Petrology, 48, 951-999.

Hinton, R.W. (1990) Ion microprobe trace-element analysis of silicates.measurement of multi-element glasses. Chemical Geology, 83, 11-25.

Always consult and cite the final, published document. See http:/www.minsocam.org or GeoscienceWorld

Holloway, J.R., and Burnham, C.W. (1972) Melting relations of basalt with equilibrium water pressure less than total pressure. Journal of Petrology, 13, 1-29.

Holland, T., and Powell, R. (2001) Calculations of phase relations involving haplogranitic melts using an internally consistent thermodynamic dataset. Journal of Petrology, 42, 673-683.

Holtz, F., Behrens, H., Dingwell, D.B., and Johannes, W. (1995) Water solubility in haplogranitc melts: compositional, pressure and temperature dependence. American Mineralogist, 80, 94-108.

Hort, M. (1998) Abrupt change in magma liquidus temperature because of volatile loss or magma mixing: effects on nucleation, crystal growth and thermal history of the magma. Journal of Petrology, 39, 1063-1076.

Huber, C., Bachmann, O., and Manga, M. (2009) Homogenization processes in silicic magma chambers by stirring and latent heat buffering. Earth and Planetary Science Letters, 283, 38-47.

Huber, C., Bachmann, O., and Manga, M. (2010) Two competing effects of volatiles on heat transfer in crystal-rich magmas: thermal insulation vs defrosting. Journal of Petrology, 51, 847-867.

Huber, C., Bachmann, O., and Dufek, J. (2011) Thermo-mechanical reactivation of locked crystal mushes: melting-induced internal fracturing and assimilation processes in magmas. Earth and Planetary Science Letters, 304, 443-454.

Humphreys, M.C.S., Edmonds, M., Christopher, T., and Hards, V. (2010) Magma hybridisation and diffusive exchange recorded in heterogeneous glasses from Soufrière Hills Volcano, Montserrat. Geophysical Research Letters, 37, L00E06.

Huppert, H.C., and Sparks, R.S.J. (1988) The fluid dynamics of crustal melting of injection of basaltic sills. Transactions of the Royal Society of Edinburgh: Earth Sciences, 79, 237-243.

Hürlimann, N., Müntener, O., Ulmer, P., Nandedkar, R., Chiaradia, M., and Ovtcharova, M. (2016) Primary magmas in continental arcs and their differentiated products: petrology of a post-plutonic dyke suite in the Tertiary Adamello Batholith (Alps). Journal of Petrology, 57, 495-534.

Jarosewich, E., Nelen, J.A., and Norberg, J.A. (1980) Reference samples for electron microprobe analysis. Geostandard Newsletter, 4, 43-47.

Jellinek, A.M., and Kerr, R.C. (1999) Mixing and compositional stratification produced by natural convection 2. Applications to the differentiation of basaltic and silicic magma chambers and komatiite lava flows. Journal of Geophysical Research, 104, 7203-7218.

Johannes, W.J., Bell, P.M., Mao, H.K., Boettcher, A.L., Chipman, D.W., Hays, J.F., Newton, R.C., and

Always consult and cite the final, published document. See http:/www.minsocam.org or GeoscienceWorld

Seifert, F. (1971) An interlaboratory comparison of piston-cylinder pressure calibration using the albite breakdown reaction. Contributions to Mineralogy and Petrology, 32, 24-38.

Johannes, W.J., and Holtz, F. (1996) Petrogenesis and Experimental Petrology of Granitic Rocks. Berlin, Springer, 335 pp.

John, B.E., and Blundy, J.D. (1993) Emplacement-related deformation of granitoidmagmas, southern Adamello Massif, Italy. Geological Society of American Bulletin, 105, 1517-1541.

Johnston, A.D., and Wyllie, P.J. (1988) Interaction of granitic and basic magmas: experimental observations on contamination processes at 10 kbar with H_2O. Contributions to Mineralogy and Petrology, 98, 352-362.

Koyaguchi, T., and Kaneko, K. (1999) A two-stage thermal evolution model of magmas in continental crust. Journal of Petrology, 40, 241-254.

Koyaguchi, T., and Kaneko, K. (2000) Thermal evolution of silicic magma chambers after basalt replenishment. Transactions of the Royal Society of Edinburgh, 91, 47-60.

Lange, R.A., and Carmichael, I.S.E. (1987) Densities of Na_2O-K_2O-CaO-MgO-FeO-Fe_2O_3-Al_2O_3-TiO_2-SiO_2 liquids: new measurements and derived partial molar properties. Geochimica et Cosmochimica Acta, 51, 2931-2946.

Lejeune, A.M., Richet, P. (1995) Rheology of crystal-bearing silicate melts: an experimental study at high viscosities. Journal of Geophysical Research, 100, 4215-4229.

Le Losq, C., Neuville, D.R., Moretti, R., and Roux, J. (2012) Determination of water content in silicate glasses using Raman spectrometry: implications for the study of explosive volcanism. American Mineralogist, 97, 779-790.

Loomis, A.A. (1963) Noritic anorthositc bodies in the Sierra Nevada Batholith. Mineralogical Society of America Special Paper, 1, 62-68.

Malfait, W.J., Seifert, R., Petitgirard, S., Perrillat, J.-P., Mezouar, M., Ota, T., Nakamura, E., Lerch, P., and Sanchez-Valle, C. (2014) Supervolcano eruptions driven by melt buoyancy in large silicic magma chambers. Nature Geoscience, 7, 122-125.

Mao, H.K., and Bell, P.M. (1971) Behavior of thermo-couples in the single-stage piston-cylinder apparatus. Carnegie Institution of Washington Yearbook, 691, 207-216.

McByrne, A.R., and Murase, T. (1984) Rheological properties of magmas. Annual Reviews of Earth and Planetary Science, 12, 337-357.

Always consult and cite the final, published document. See http:/www.minsocam.org or GeoscienceWorld

McDade, P., Wood, B.J., van Westrenen, W., Brooker, R.A., Gudmudsson, G., Soulard, H., Najorka, J., and Blundy, J.D. (2002) Pressure corrections for a selection of piston-cylinder cell assemblies. Mineralogical Magazine, 66, 1021-1028.

Merrill, R.B., and Wyllie, P.J. (1975) Kaersutite and kaersutite eclogite from Kakanui, New Zealand: water excess and water deficient melting to 30 kilobars. Geological Society of American Bulletin, 86, 555-570.

Moore, J.G., and Lockwood, J.P. (1973) Origin of comb layering and orbicular structure, Sierra Nevada Batholith, California. Geological Society of American Bulletin, 84, 1-20.

Murphy, M.D., Sparks, R.S.J., Barclay, J., Carroll, M.R., Brewer, T.S. (2000) Remobilization of andesite magma by intrusion of mafic magma at the Soufriere Hills Volcano, Montserrat, West Indies. Journal of Petrology, 41, 21-42.

Ni, H., and Zhang, Y. (2008) H_2O diffusion models in rhyolitic melt with new high pressure data. Chemical Geology, 250, 68-78.

Ochs, F.A., and Lange, R.A. (1999) The density of hydrous magmatic liquids. Science, 283, 1314-1317.

Parmigiani, A., Huber, C., and Bachmann, O. (2014) Mush microphysics and the reactivation of crystal-rich magma reservoirs. Journal of Geophysical Research, 119, doi:10.1002/2014JB011124.

Parmigiani, A., Faroughi S, Huber, C., Bachmann, O., and Su, Y. (2016) Bubble accumulation and its role in the evolution of magma reservoirs in the upper crust. Nature, 532, 492-495.

Paterson, S.R., Okaya, D., Memeti, V., Economos, R., and Miller, R.B. (2011) Magma addition and flux calculations of incrementally constructed magma chambers in continental margin arcs: combined field, geochronologic, and thermal modeling studies. Geosphere, 7, 1439-1468.

Paterson, S.R., and Ducea, M.N. (2015) Arc Magmatic Tempos. Elements, 11, 155 pp.

Petford, N. (2003) Rheology of granitic magmas during ascent and emplacement. Annual Reviews of Fluid Mechanics, 31, 399-427.

Plank, T., Kelley, K.A., Zimmer, M.M., Hauri, E.H., and Wallace, P.J. (2013) Why do mafic arc magmas contain ~4 wt% water on average? Earth and Planetary Science Letters, 364, 168-179.

Pistone, M., Caricchi, L., Ulmer, P., Burlini, L., Ardia, P., Reusser, E., Marone, F., and Arbaret, L. (2012) Deformation experiments of bubble- and crystal-bearing magmas: rheological and microstructural analysis. Journal of Geophysical Research, 117, doi:10.1029/2011JB008986.

Always consult and cite the final, published document. See http:/www.minsocam.org or GeoscienceWorld

Pistone, M., Caricchi, L., Ulmer, P., Reusser, E., and Ardia, P. (2013) Rheology of volatile-bearing crystal mushes: mobilization vs. viscous death. Chemical Geology, 345, 16-39.

Pistone, M., Arzilli, F., Dobson, K.J., Cordonnier, B., Reusser, E., Ulmer, P., Marone, F., Whittington, A.G., Mancini, L., Fife, J.L., and Blundy, J.D. (2015) Gas-driven filter pressing in magmas: insights into in-situ melt segregation from crystal mushes. Geology, 43, 699-702.

Pistone, M., Blundy, J.D., Brooker, R.A., and EIMF (2016) Textural and chemical consequences of interaction between hydrous mafic and felsic magmas: an experimental study. Contributions to Mineralogy and Petrology, 171, doi10.1007/s00410-015-1218-4.

Podladchikov, Y.Y., and Wickham, M. (1994) Crystallization of hydrous magmas: calculations of associated thermal effects, volatile fluxes, and isotopic alteration. Journal of Geology, 102, 25-45.

Poldervaart, A., and Taubeneck, W.H. (1959) Layered intrusions of the Willow Lake type. Geological Society of American Bulletin, 70, 1395-1398.

Poli, S., and Schmidt, M.W. (1995) H_2O transport and release in subduction zones: experimental constraints on basaltic and andesitic systems. Journal of Geophysical Research, 100, 22299-22314.

Romine, W.L., Whittington, A.G., Nabelek, P.I., Hofmeister, A.M. (2012) Thermal diffusivity of rhyolitic glasses and melts: effects of temperature, crystals and dissolved water. Bulletin of Volcanology, 74, 2273-2287.

Saunders, K.E., Buse, B., Kilburn, M., Kearns, S., Blundy, J.D. (2014) Nanoscale characterisation of crystal zoning. Chem Geology, 364, 20-32.

Schmidt, M.W., Poli, S. (1998) Experimentally based water budgets for dehydrating slabs and consequences for arc magma generation. Earth and Planetary Science Letters, 163, 361-379.

Seaman, S.J., and Ramsey, P.C. (1992) Effects of magma mingling in the granites of Mount Desert Island, Maine. Journal of Geology, 100, 395-409.

Shannon, J.R., Walker, B.M., Carten, R.B., and Geraghty, E.P. (1982) Unidirectional solidification textures and their significance in determining relative ages of intrusions at the Henderson Mine, Colorado. Geology, 10, 293-297.

Sigmundsson, F., Hreinsdóttir, S., Hooper, A., Árnadóttir, T., Pedersen, R., Roberts, M.J., Óskarsson, N., Auriac, A., Decriem, J., Einarsson, P., Geirsson, H., Hensch, M., Ófeigsson, B.G., Sturkell, E., Sveinbjörnsson, H., and Feigl, K.L. (2010) Intrusion triggering of the 2010 Eyjafjallajökull explosive eruption. Nature, 468, 426-430.

Always consult and cite the final, published document. See http:/www.minsocam.org or GeoscienceWorld

Sisson, T.W., Grove, T.L., and Coleman D.S. (1996) Hornblende gabbro sill complex at Onion Valley, California, and a mixing origin for the Sierra Nevada batholith. Contributions to Mineralogy and Petrology, 126, 81-108.

Sisson, T.W., and Bacon, C.R. (1999) Gas-driven filter pressing in magmas. Geology, 27, 613-616.

Solano, J.M.S., Jackson, M.D., Sparks, R.S.J., Blundy, J.D., and Annen, C. (2012) Melt segregation in deep crustal hot zones: a mechanism for chemical differentiation, crustal assimilation and the formation of evolved magmas. Journal of Petrology, 53, 1999-2026.

Suzuki, Y., and Nakada, S. (2007) Remobilization of highly crystalline felsic magma by injection of mafic magma: constraints from the middle sixth century eruption at Haruna Volcano, Honshu, Japan. Journal of Petrology, 48, 1543-1567.

Takahashi, N., Kodaira, S., Klemperer, S.L., Tatsumi, Y., Kaneda, Y., and Suyehiro, K. (2007) Crustal structure and evolution of the Mariana intra-oceanic island arc. Geology, 35, 203-206.

Tapster, S., Condon, D.J., Naden, J., Noble, S.R., Petterson, M.G., Roberts, N.M.W., Saunders, A.D., and Smith, D.J. (2016) Rapid thermal rejuvenation of high-crystallinity magma linked to porphyry copper deposit formation; evidence from the Koloula Porphyry Prospect, Solomon Islands. Earth and Planetary Science Letters, 442, 206-217.

Tatsumi, Y. (2000) Continental crust formation by crustal delamination in subduction zones and complementary accumulation of the enriched mantle component in the mantle. Geochemistry, Geophysics, Geosystems, 1, doi:10.1029/2000GC000094.

Tomiya, A., Miyagi, I., Saito, G., and Geshi, N. (2013) Short time scales of magma-mixing processes prior to the 2011 eruption of Shinmoedake volcano, Kirishima volcanic group, Japan. Bulletin of Volcanology, 7, 750-768.

Trigila, R., Battaglia, M., Sottili, G., and Brilli, M. (2008) Volcanic eruptions from ghost magma chambers. Geophysical Research Letters, 35, doi:10.1029/2008GL034579.

Tuttle, O.F., and Bowen, N.L. (1958) Origin of granite in the light of experimental studies in the system $NaAlSi_3O_8$-$KAlSi_3O_8$-SiO_2-H_2O. Geological Society of Amerca Memoire, 74, 153 pp.

Ulmer, P. (1988) High Pressure Phase Equilibria of a calc-alkaline picro-basalt: implications for the genesis of calc-alkaline magmas. Carnegie Institution of Washington Yearbook, Annual Report of the Director of the Geophysical Laboratory, 88, 28-35.

Ulmer, P. (2001) Partial melting in the mantle wedge: the role of H_2O in the genesis of mantle-derived

Always consult and cite the final, published document. See http:/www.minsocam.org or GeoscienceWorld

"arc-related" magmas. Physics and Earth Planetary Interiors, 127, 215-232.

Ulmer, P. (2007) Differentiation of mantle-derived calc-alkaline magmas at mid to lower crustal levels: experimental and petrologic constraints. Periodico di Mineralogia, 76, 309-325.

Ulmer, P., Callegari, E., and Sonderegger, U.C. (1983) Genesis of the mafic rocks and their genetical relations to the tonalitic–trondhjemitic granitoids of the southern part of the Adamello Batholith (Northern Italy). Memorie della Società Geologica Italiana, 26, 171-222.

Ulmer, P., and Trommsdorff, V. (1995) Serpentine stability to mantle depth and subduction related magmatism. Science, 268, 858-861.

van der Laan, S.R., and Wyllie, P.J. (1993) Experimental interaction of granitic and basaltic magmas and implications for mafic enclaves. Journal of Petrology, 34, 491-517.

Verberne, R., Ulmer, P., and Müntener, O. (2011) Field relations and consequences for emplacement of the Listino Ring Structure, Adamello Massif, N-Italy, Abstract Volume 9th Swiss Geoscience Meeting.

Watson, E.B. (1982) Basaltic contamination by continental crust: some experiments and models. Contributions to Mineralogy and Petrology, 80, 73-87.

Wyllie, P.J., Cox, K.G., and Biggar, G.M. (1962) The habit of apatite in synthetic systems and igneous rocks. Journal of Petrology, 3, 238-243.

Yoder, H.S.Jr., and Tilley, C.E. (1962) Origin of basalt magmas: an experimental study of natural and synthetic rock systems. Journal of Petrology 3, 342-532.

Yoder, H.S. Jr. (1973) Contemporaneous basaltic and rhyolitic magmas. American Mineralogist, 58, 153-171.

Yoder, H.S. Jr., Stewart, D.B., and Smith, J.R. (1957) Ternary feldspars. Carnegie Institution of Washington Year book, 55, 206-214.

FIGURE CAPTIONS

Figure 1: Example of textures associated with hydrous mafic magmas from the Tertiary Adamello Batholith (Alps, Italy). A) Polished rock slab from the Val Fredda Complex (Blundy and Sparks 1992) showing interaction between a hot (1050 °C) hornblende-rich gabbro (lower dark portion) ascending from the deep crust (7 kbar; Ulmer 1988; 2007; Ulmer et al. 1983) and relatively cool (850 °C), partially molten, tonalite host (upper lighter portion) emplaced at shallow depth (2-3 kbar; Blundy and

Always consult and cite the final, published document. See http:/www.minsocam.org or GeoscienceWorld

Sparks 1992). The interaction between the two rocks is marked by a fine-grained "chilled margin" to the gabbro at 950 °C (i.e., equilibrium temperature after heat diffusion). Wisps of solidified mafic magma can be seen rising from the interface and permeating the tonalite, which is rendered anomalously darker as a consequence. Rounded, grey quartz phenocrysts in the tonalite have developed hornblende-bearing coronas as a consequence of interaction with mafic magma. The white dashed line outlines the contact between tonalite and gabbro. B) Binary image of the polished rock slab in A showing original whitish minerals in black (i.e., quartz in tonalite and plagioclase in gabbro) and dark/green hornblende in white. The binary image is obtained using the open-source Java image processing software ImageJ v1.4. Light blue thick arrows highlight potential water movement by diffusion and/or exsolution from gabbro to tonalite as revealed by green hornblende in A (white minerals in tonalite in B) and quartz crystal size reduction in the tonalite portions characterised by abundant hornblende. The red dashed line outlines the contact between tonalite and gabbro.

Figure 2: Microstructural and chemical (i.e., H_2O content in the glass) characterisation of experimental run products. ***A-C)*** BSE image detailing the sample-sample interaction interface of the run products: ***A)*** F50-M (Setup A); ***B)*** F60-M-F60 (Setup B); ***C)*** F70-M (Setup A). The yellow solid (i.e., data-supported) and dashed (i.e., interpreted) arrows indicate directions of H_2O movement in the dacite domain; SIMS-based H_2O content values (in yellow) are in wt% and refer to single analytical spots and average of two or more data analysis spots in the same sample location (highlighted by the curved yellow lines). The white dashed lines show the sample-sample interface. The black scale bar is 1 mm. The red square highlights the image inset in A. ***D)*** BSE image showing representative FEG-EPMA-based analysis spots (black dots) reporting SiO_2 content across quartz crystal and surrounding glass in run product F70-M. The black scale bar is 7 µm. ***E)*** Raman-based OH-intensity map, acquired in the range of 1384 to 1412 cm^{-1}, showing H_2O contents in run product F50-M. The white scale bar is 100 µm in ***E***. The colour scale in ***E***, calibrated with SIMS-based H_2O contents in the residual glass (see white dots with corresponding local H_2O contents), shows H_2O content values in wt%. The yellow dashed line in ***E*** highlights the sample-sample interface. In all panels ***A-E*** the following phases are present: vesicles (black circles), hornblende (very light grey objects in M and white objects close to quartz crystals in F50), plagioclase (light grey), oxides (white), quartz (very dark grey), and silicic glass (dark grey matrix).

Always consult and cite the final, published document. See http:/www.minsocam.org or GeoscienceWorld

Figure 3: SIMS-based H_2O contents in the interstitial glass (black circles) and calculated bulk H_2O (open circles) across different run products. Data are displayed according to the orthogonal distance of the analysis spots from the interface(s) between samples (displayed as horizontal black solid lines with opposing arrows). Vertical black dashed lines represent starting H_2O contents in the glass of dacite and andesite samples. Grey scale areas indicate different crystal fractions (ϕ, darker area = larger crystallinity) in dacite and andesite. Large black solid arrows indicate directions of H_2O movement during interaction.

Figure 4: Pressure-temperature plot showing H_2O-saturated (wet) liquidus and solidus temperatures (black solid curves) and contours of H_2O solubility increasing with pressure/depth (dashed lines) in haplogranite melts based on the experimental data of Holtz et al. (1995) and the phase relation calculations of Holland and Powell (2001). Despite the compositional differences between haplogranite (Holtz et al. 1995) and rhyolite melts (this study), this diagram can be applied generally to high-silica systems (> 65 wt% SiO_2). This plot illustrates the effect of coupled heat and water diffusion from the hot (1050 °C) crystal-poor gabbroic magma (white star), ascending adiabatically from the deep crust (7 kbar; Ulmer 1988; 2007; Ulmer et al. 1983) into the original crystal-rich (> 70 vol% crystals) host tonalite (850 °C; 4 kbar, based on the experiments of this study; black star). The mafic-felsic interaction heats the tonalite system to increase to 950 °C (yellow star; Blundy and Sparks 1992) and drives partial melting by heat diffusion (A). The addition of H_2O suppresses the liquidus and solidus temperature (i.e., liquidus temperature down to 800 °C, with an average value of 860 °C; Pistone et al. 2016), further increasing the melting of the tonalite under isothermal conditions (B). Thick dashed lines depict different crystal fractions (ϕ) of the host tonalite. H_2O-free (dry) liquidi and solidi are reported for reference. The mafic magma (white star) is reported in A for reference; but this composition is characterised by different phase relations, including liquidi and solidi, which are not shown here. The qualitative sketch (redrawn after Pistone et al. 2013) shows an upper crystal-rich felsic pluton underplated by a hot mafic magma releasing heat and water into the felsic host (see black arrows). In this sketch gas exsolution is expected at the interface when the residual melt is H_2O-saturated as observed in the run products (see inset image in Figure 2A).

Always consult and cite the final, published document. See http:/www.minsocam.org or GeoscienceWorld

Figure 5: Melt density (ρ_{melt}) profiles within the experimental charges from this study. ρ_{melt} values of the residual glass in the dacite and andesite were estimated using a combination of EPMA-based glass chemistry, SIMS-based H_2O data and the model of Lange and Carmichael (1987). Crystal fraction values and symbols as in Figure 2.

Figure 6: Logarithm of melt viscosity (η_{melt}) profiles within the experimental charges from this study. η_{melt} values of the residual glass in the dacite and andesite were estimated using a combination of the EPMA-based glass chemistry, SIMS-based H_2O data and the model of Giordano et al. (2008), which is calibrated at 1 bar (black circles). A correction factor of 1.8 log units in η_{melt} due to the pressure effect on η_{melt} (Ardia et al. 2008; 2014; Pistone et al. 2012; P-η_{melt}) is applied (open circles). Crystal fraction values and symbols as in Figure 2.

Figure 7: Log-time required to extract silicic melt from a crystal mush a function of crystal fraction (ϕ). The light and dark grey rectangles indicate the average residence times of crystal mushes (10^4-10^5 years; Bachmann and Bergantz 2004, and references therein) and those of long-lived plutons in the Earth's crust (Glazner et al. 2004). Water diffusion timescale (see double arrows) is calculated using the simple approximation: $x = \sqrt{t \times D_{H_2O}}$, (Watson 1982; Baker 1991; with $D_{H_2O} = 3 \cdot 10^{-10}$ m^2/s; Ni and Zhang (2008), and t = experimental duration), a length scale ranging from 5 to 25 m based on the length scale of the leucogranite dikes (i.e., extracted melt from the Monoccola Granodiorite mush) observed in the Listino Ring Complex in Adamello Massif, Italy (Verberne et al. 2011). Above the crystal maximum packing fraction (ϕ_{max} = 0.64), melt extraction ceases.

Always consult and cite the final, published document. See http:/www.minsocam.org or GeoscienceWorld

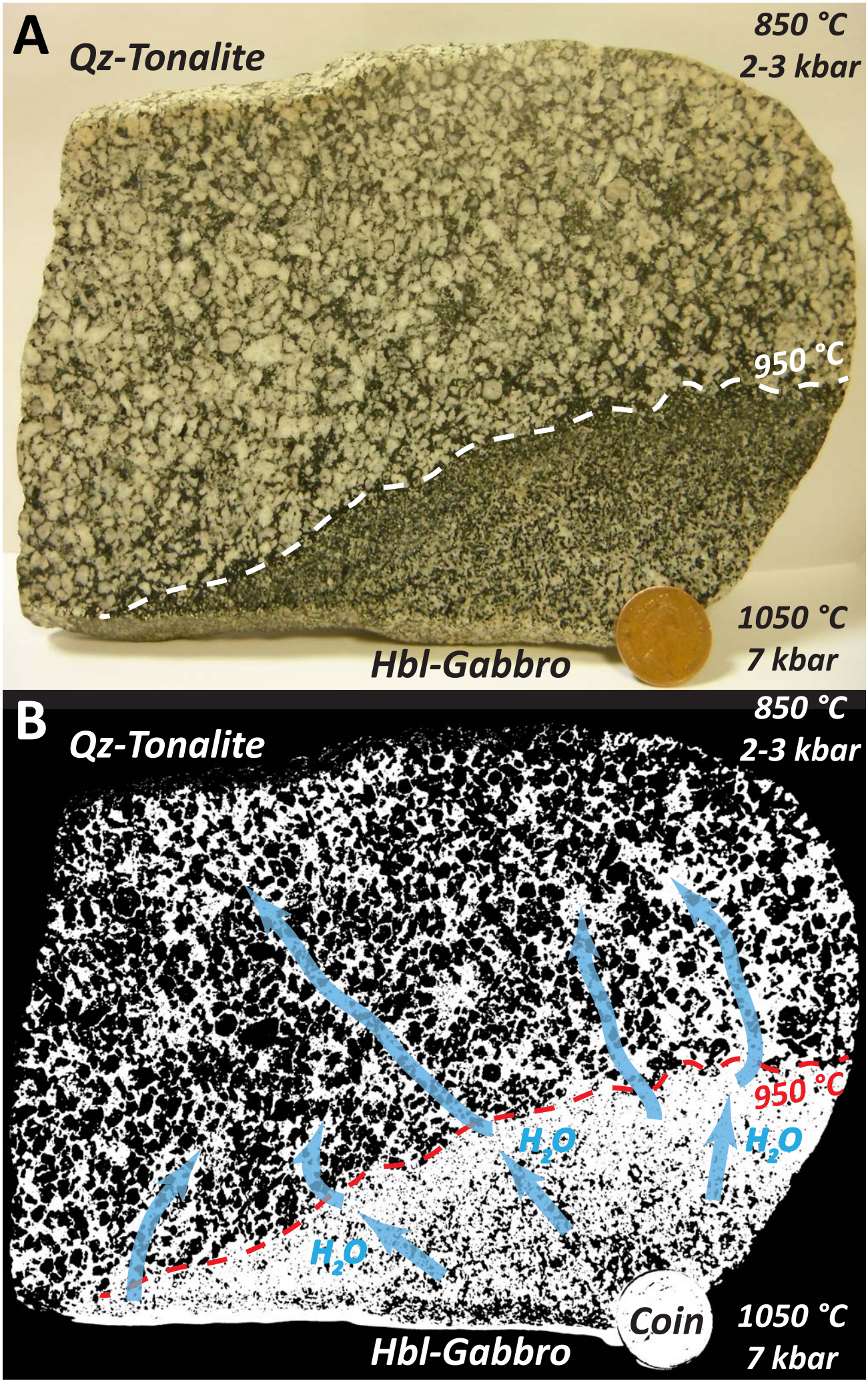
A
Qz-Tonalite
850 °C
2-3 kbar
950 °C
1050 °C
7 kbar
Hbl-Gabbro
B
Qz-Tonalite
850 °C
2-3 kbar
950 °C
H_2O
H_2O
H_2O
Coin
1050 °C
7 kbar
Hbl-Gabbro

Figure 1

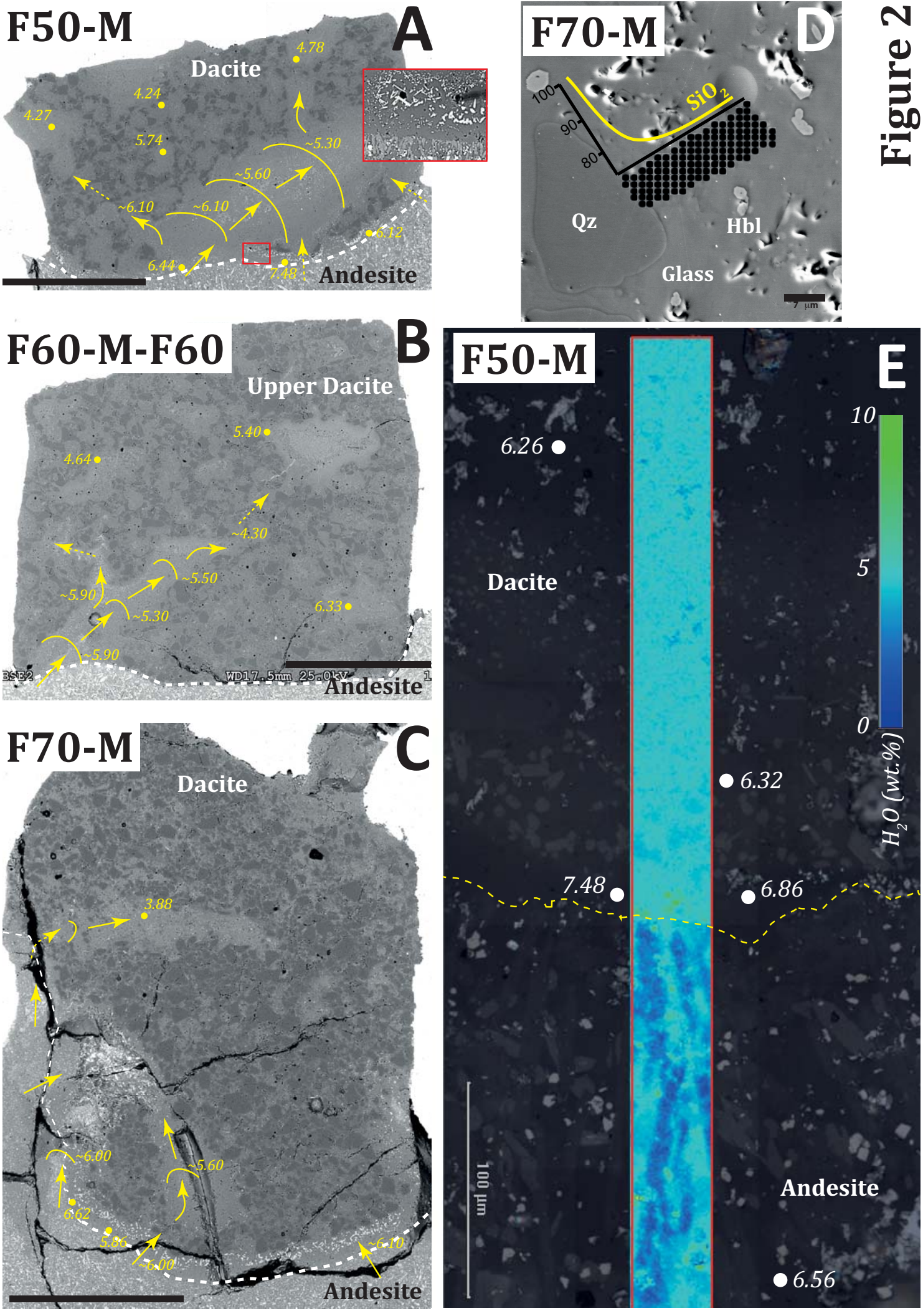
F50-M
A
Dacite
4.78
4.24
4.27
5.74
~5.30
~5.60
~6.10
~6.10
6.12
6.44
7.48
Andesite
F70-M
D
100
90
80
SiO2
Qz
Hbl
Glass
F60-M-F60
B
Upper Dacite
5.40
4.64
~4.30
~5.50
~5.90
~5.30
6.33
~5.90
Andesite
F70-M
C
Dacite
3.88
~6.00
~5.60
6.62
5.86
~6.00
~6.10
Andesite
F50-M
E
10
5
0
H2O (wt.%)
6.26
Dacite
6.32
7.48
6.86
100 µm
Andesite
6.56

Figure 2

Figure 3

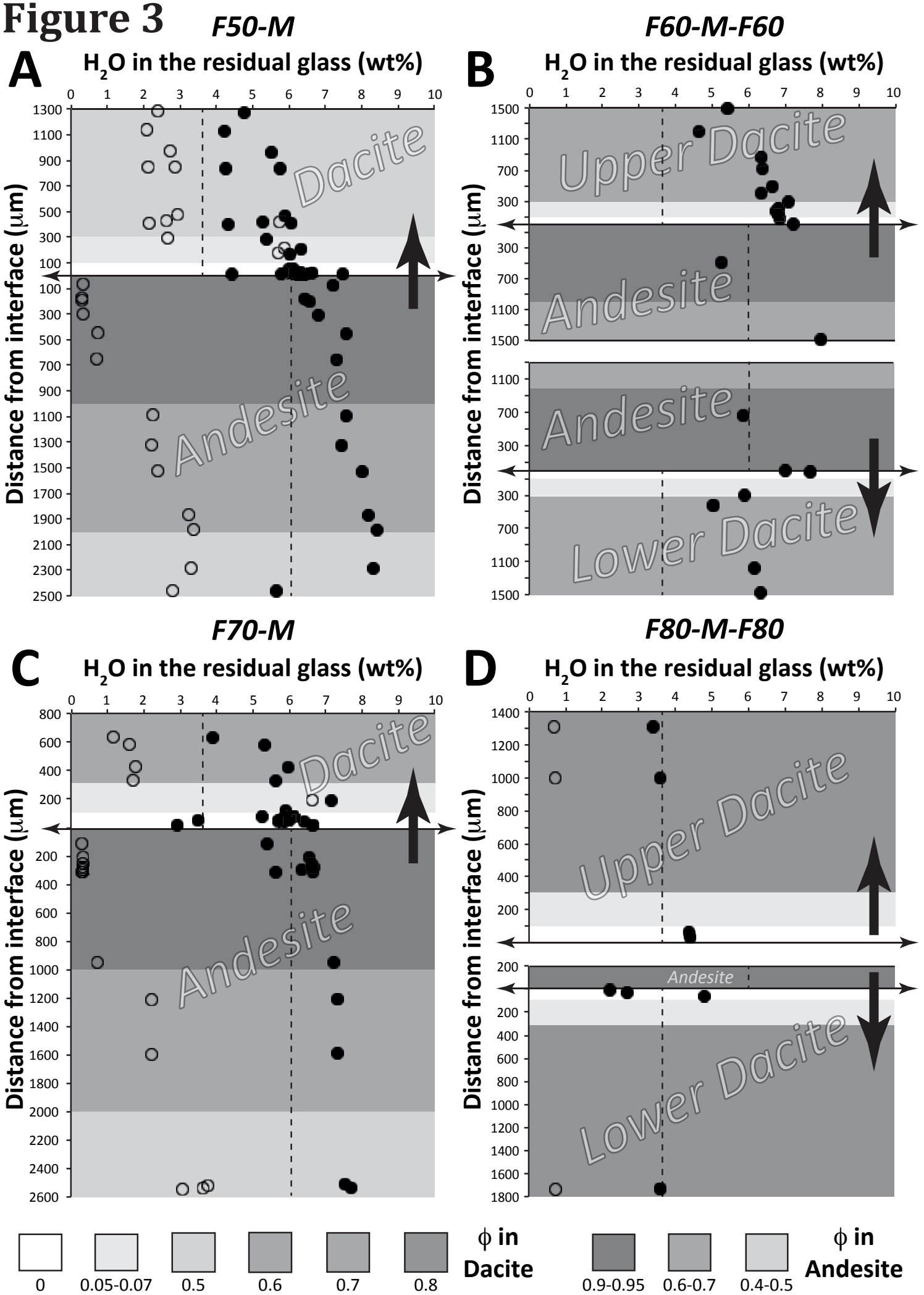
F50-M
A
H2O in the residual glass (wt%)
Distance from interface (μm)
Dacite
Andesite
F60-M-F60
B
H2O in the residual glass (wt%)
Distance from interface (μm)
Upper Dacite
Andesite
Andesite
Lower Dacite
F70-M
C
H2O in the residual glass (wt%)
Distance from interface (μm)
Dacite
Andesite
F80-M-F80
D
H2O in the residual glass (wt%)
Distance from interface (μm)
Upper Dacite
Andesite
Lower Dacite
0
0.05-0.07
0.5
0.6
0.7
0.8
ϕ in Dacite
0.9-0.95
0.6-0.7
0.4-0.5
ϕ in Andesite

Figure 4

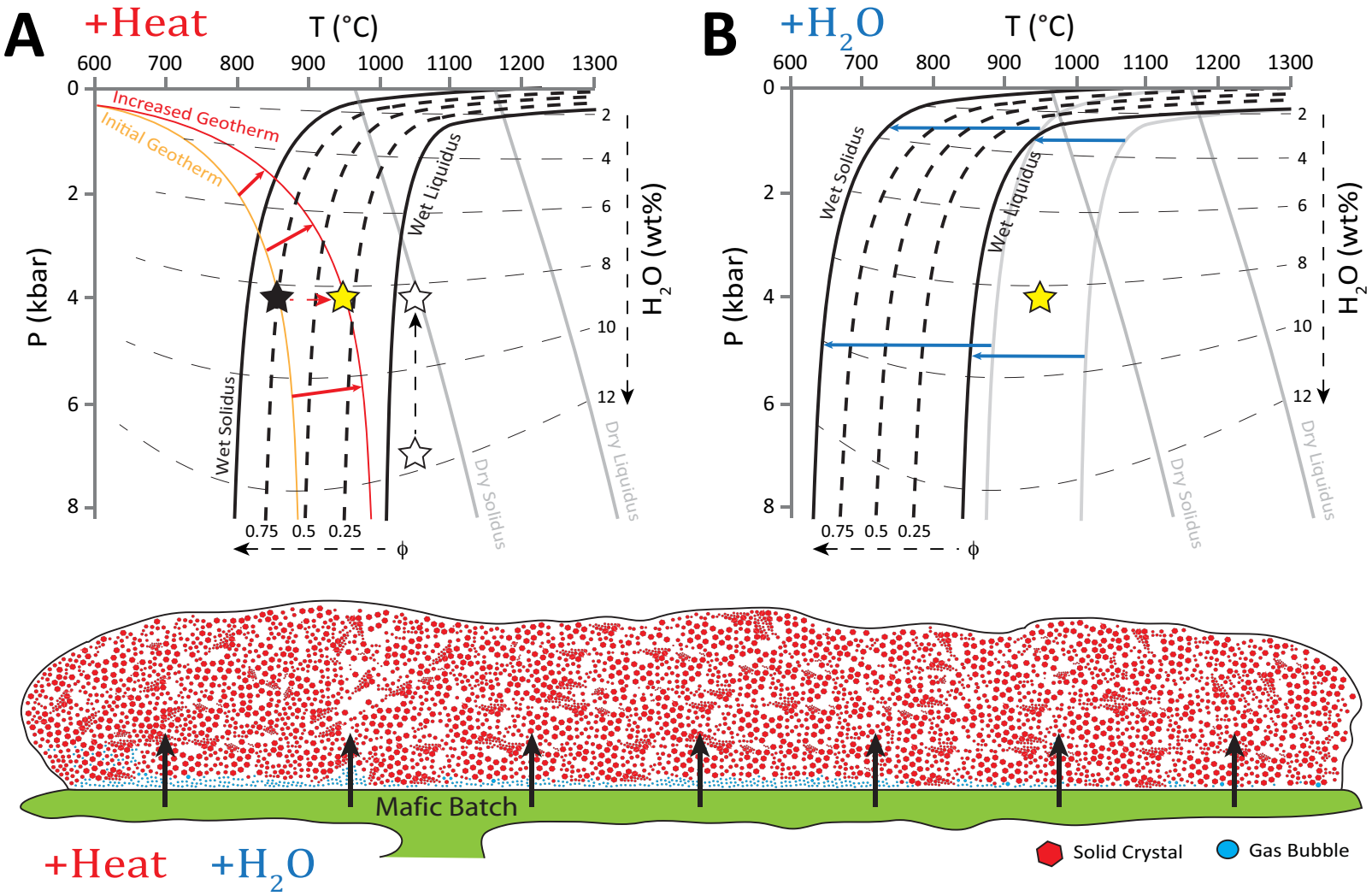
A
+Heat
T (°C)
600 700 800 900 1000 1100 1200 1300
P (kbar)
0 2 4 6 8
Increased Geotherm
Initial Geotherm
Wet Solidus
Wet Liquidus
Dry Solidus
Dry Liquidus
2 4 6 8 10 12
H_2O (wt%)
0.75 0.5 0.25
ϕ
B
+H_2O
T (°C)
600 700 800 900 1000 1100 1200 1300
P (kbar)
0 2 4 6 8
Wet Solidus
Wet Liquidus
Dry Solidus
Dry Liquidus
2 4 6 8 10 12
H_2O (wt%)
0.75 0.5 0.25
ϕ
Mafic Batch
+Heat
+H_2O
Solid Crystal
Gas Bubble

Figure 5

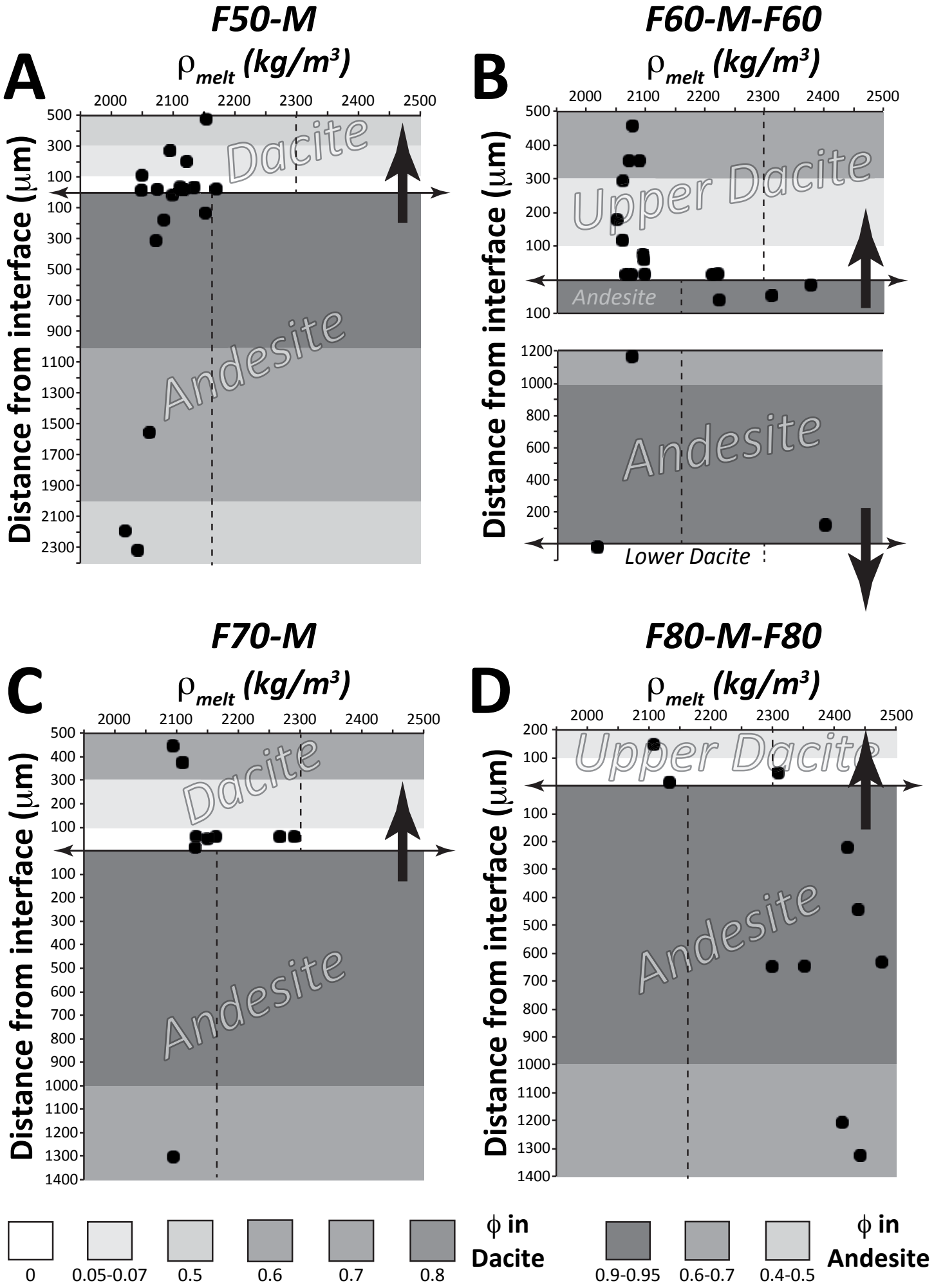
F50-M
A
ρ_{melt} (kg/m³)
Distance from interface (μm)
Dacite
Andesite
F60-M-F60
B
Upper Dacite
Andesite
Lower Dacite
F70-M
C
Dacite
Andesite
F80-M-F80
D
Upper Dacite
Andesite
ϕ in Dacite
0
0.05-0.07
0.5
0.6
0.7
0.8
ϕ in Andesite
0.9-0.95
0.6-0.7
0.4-0.5

Figure 6

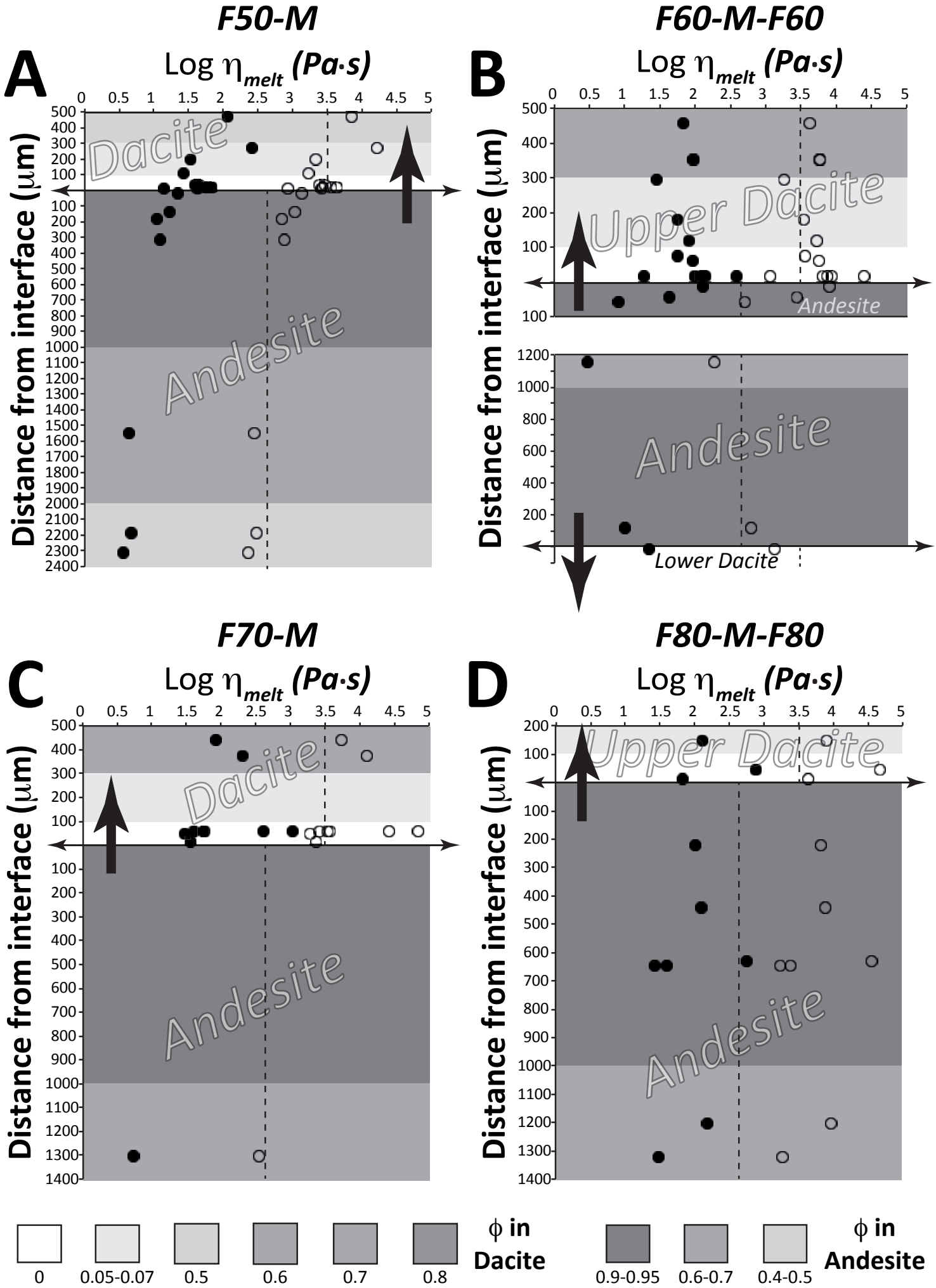
F50-M
A
Log η melt (Pa·s)
Distance from interface (μm)
Dacite
Andesite
F60-M-F60
B
Log η melt (Pa·s)
Distance from interface (μm)
Upper Dacite
Andesite
Andesite
Lower Dacite
F70-M
C
Log η melt (Pa·s)
Distance from interface (μm)
Dacite
Andesite
F80-M-F80
D
Log η melt (Pa·s)
Distance from interface (μm)
Upper Dacite
Andesite
0
0.05-0.07
0.5
0.6
0.7
0.8
ϕ in Dacite
0.9-0.95
0.6-0.7
0.4-0.5
ϕ in Andesite

Figure 7

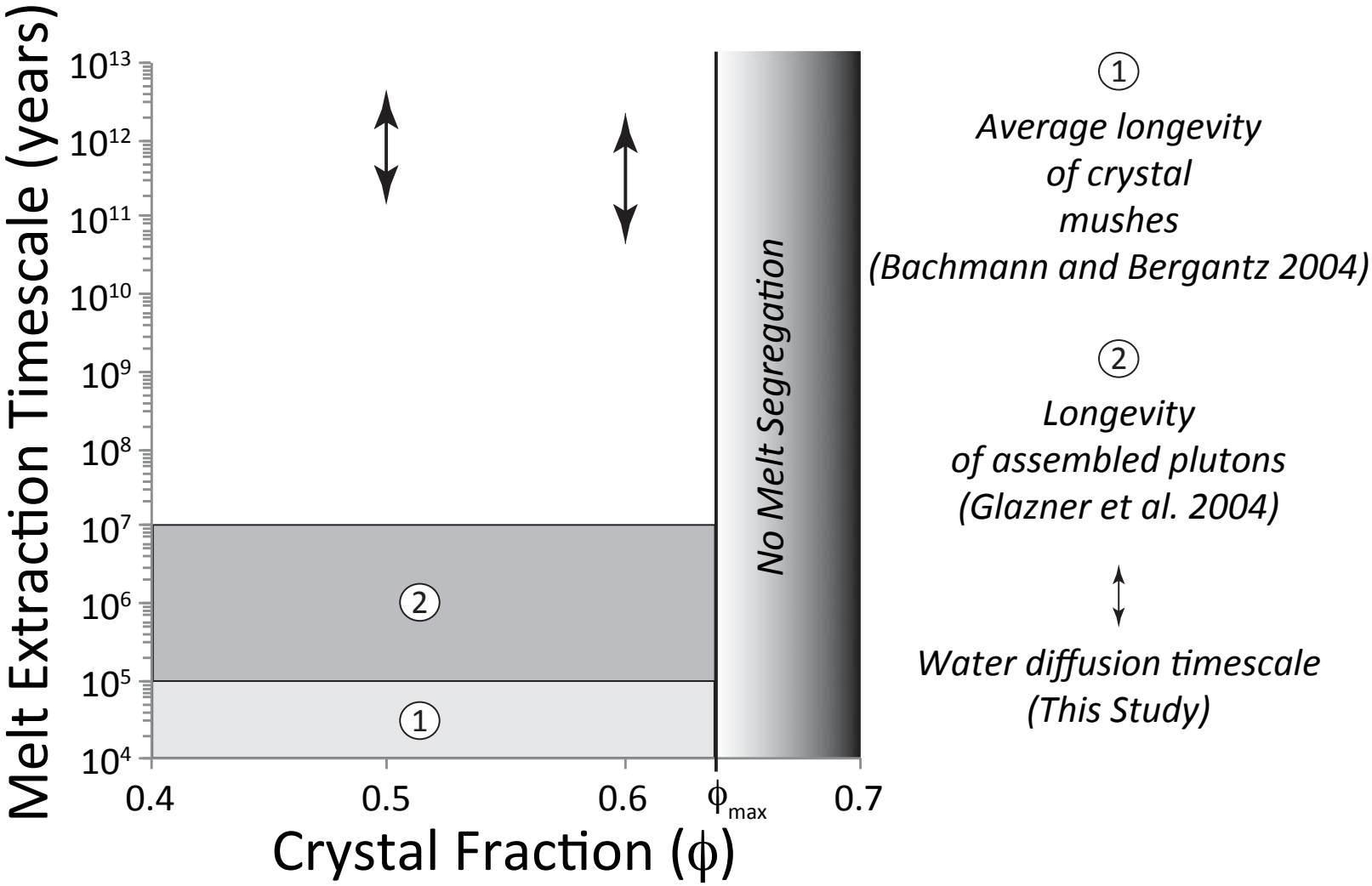
Melt Extraction Timescale (years)
10^{13}
10^{12}
10^{11}
10^{10}
10^{9}
10^{8}
10^{7}
10^{6}
10^{5}
10^{4}
0.4
0.5
0.6
ϕ_{max}
0.7
Crystal Fraction (ϕ)
No Melt Segregation
2
1
1
Average longevity of crystal mushes (Bachmann and Bergantz 2004)
2
Longevity of assembled plutons (Glazner et al. 2004)
Water diffusion timescale (This Study)